Materials Research Proceedings 41 (2024) 2400-2409 https://doi.org/10.21741/9781644903131-264

Simulation-based analysis of electrical current induction in a device for electrochemical precision machining of Nd-Fe-B permanent magnets

THIELECKE Alexander[1,a *], HACKERT-OSCHÄTZCHEN Matthias[1,b], MEICHSNER Gunnar[1,c], BERGER Thomas[2,d], LOEBEL Sascha[2,e], MARTIN André[2,f], SCHULZE Robin[3,g], SCHUBERT Andreas[2,h]

[1]Chair of Manufacturing Technology with Focus Machining, Faculty of Mechanical Engineering, Otto von Guericke University Magdeburg, Universitätsplatz 2, 39106 Magdeburg, Germany

[2]Professorship Micromanufacturing Technology, Chemnitz University of Technology, 09107 Chemnitz, Germany

[3]SITEC Industrietechnologie GmbH, 09114 Chemnitz, Germany

[a]alexander.thielecke@ovgu.de, [b]matthias.hackert-oschaetzchen@ovgu.de, [c]gunnar.meichsner@ovgu.de, [d]thomas.berger@mb.tu-chemnitz.de, [e]sascha.loebel@mb.tu-chemnitz.de, [f]andre.martin@mb.tu-chemnitz.de, [g]robin.schulze@sitec-technology.de, [h]andreas.schubert@mb.tu-chemnitz.de

Keywords: Electrochemical Machining, Permanent Magnets, Multiphysics Simulation

Abstract. Sintered permanent magnets, consisting of the neodymium-iron-boron (Nd-Fe-B) alloy, are installed as rotor magnets in small and precision electric drives due to their high magnetic forces in small volumes. When permanent magnets are brought into their final shape by electrical discharge machining (EDM), the thermal influence of this manufacturing process has negative effects on the magnetic properties of the workpieces. In consequence, re-magnetization of the workpieces is necessary after the finishing process. As an alternative manufacturing technology, electrochemical precision machining with an oscillating electrode and pulsed direct current (PECM) has the potential to eliminate this subsequent processing step. Based on Faraday's law of induction, an electrical induction current is expected to be generated by the cathode oscillation during the manufacturing process. In this study, the effect of the magnetic field of the workpiece on the process current and on the ablation-effective local electrical current density of the PECM process is analyzed based on multiphysics simulation.

Introduction

Permanent magnets are used as rotor magnets for small or precision drives with two degrees of freedom. These permanent magnets are installed in pairs due to the required degrees of freedom and are, for instance, double spherical in shape. High-performance Nd-Fe-B alloys are applied as the material for the rotor magnets. One of the factors that determines the extent to which undesirable cogging torques of the electric drive result is the shape of the rotor magnets, which makes precise machining of these permanent magnets essential.

After the sintered permanent magnets have been machined into their final shape using EDM, a subsequent magnetization process of the components is required [1]. The additional process step is necessary because the Nd-Fe-B materials are characterized by low application temperatures, so that temperatures above 80 °C are expected to affect the magnetization [2]. PECM offers an alternative finishing process without re-magnetizing the components after shaping. Compared to EDM, PECM machining takes place in an aqueous electrolyte solution, which is usually pre-tempered to less than 30 °C and only heats up slightly during the machining process. As a result,

only minor thermal effects occur, which are expected to not affect the magnetic properties of the components. The PECM principle is illustrated in Fig. 1.

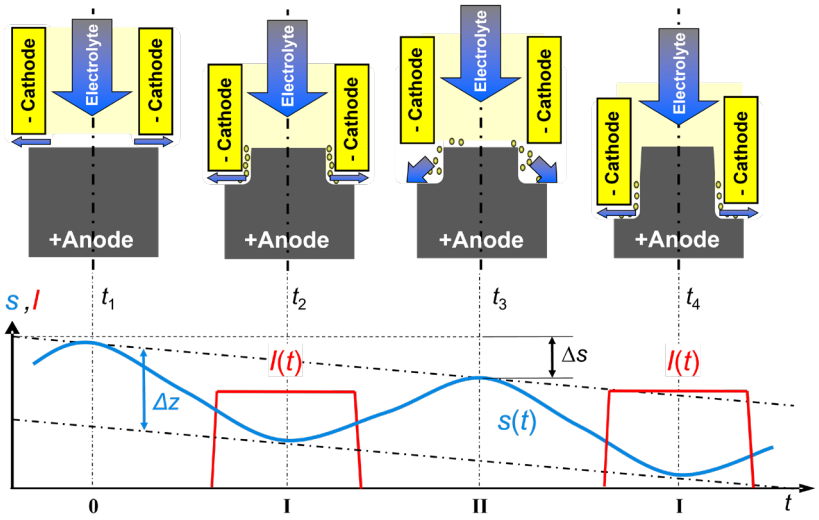

Figure 1 – Principle of ECM with pulsed direct current and an oscillating cathode according to [3]

During electrochemical machining, the gas concentration and the degree of contamination of the electrolyte increase in the working gap. This results in a reduction in the reaction components of the electrolyte and consequently a decrease in electrical conductivity. To prevent this negative effect, pulsation of the current is used in the PECM process. This allows fresh electrolyte to flow into the process area during the pulse interruption. With PECM, the current pulse is often combined with an oscillation of the cathode in order to achieve an even stronger localization of the current density and thus an even higher accuracy of the workpiece shape.

In a previous study was shown that the oscillating movement of the cathode causes an electrical current induction in form of eddy currents during the PECM process in a rotationally symmetrical workpiece and in a rotationally symmetrical cathode [4]. Circular eddy currents are induction currents that are induced in an electrically conductive material in a magnetic field that changes over time or in a moving electrically conductive material in a magnetic field that remains constant over time. The interaction between the electric and magnetic fields that lead to current induction can be explained by the differential form of Faraday's law of electromagnetic induction in Eq. 1 [5].

$$\nabla \times \vec{E} = -\frac{\partial \vec{\mathrm{B}}}{\partial \mathrm{t}} \tag{1}$$

Eq. 1 states that a time-varying magnetic field is accompanied by a spatially varying electric field and vice versa. Where E represents the electric field, B the magnetic field and ∇x the curl operator. In this study the effect of electrical current induction on the initial state and during the machining of the spherical shape of a rotor magnet is to be analyzed using 2 transient simulation models with the commercial FEM software *COMSOL Multiphysics*.

Model description

Geometry and material parameters

The PECM device shown in previous experiments is designed for 2-sided machining of the rotor magnets [6]. In the first step, the concave surface is machined. In the second step, the component is re-clamped to machine the convex shape. The dimensions of the workpiece are shown in Fig. 2.

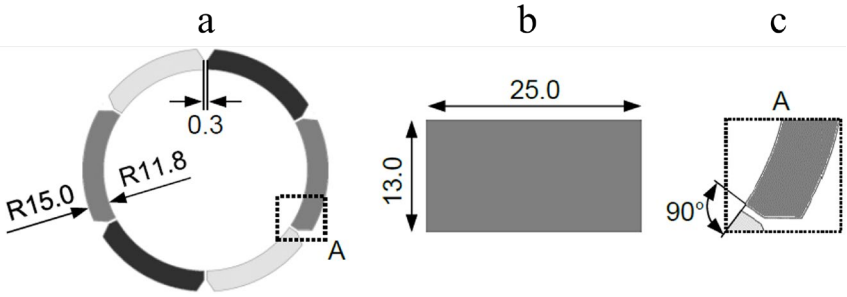

Figure 2 – Cross-sectional view of a rotary drive with three terminal pairs (a), top view of a single rotor magnet (b) and detailed cross-sectional view (c); dimensions in mm [6]

To investigate if the different shapes of the workpiece during the PECM process have a different effect on the strength and distribution of the induced eddy currents, 2 transient 2D simulation models were set up to analyze the induced current. Fig. 3 shows the 2 different machining stages of the first step of the machining process.

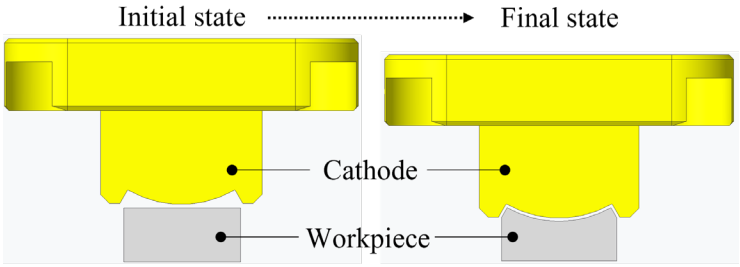

Figure 3 – Initial- and processing states of the workpiece in the PECM process

The design of the model geometries, material data and PECM input parameters were derived from previously performed experiments [6]. In the following, the geometry representing the workpiece in its initial state is referred to as “Model initial state” and the machined workpiece as “Model final state”. As an example, the 2D model geometry of Model initial state derived from the cross-section of the PECM device, is shown in Fig. 4.

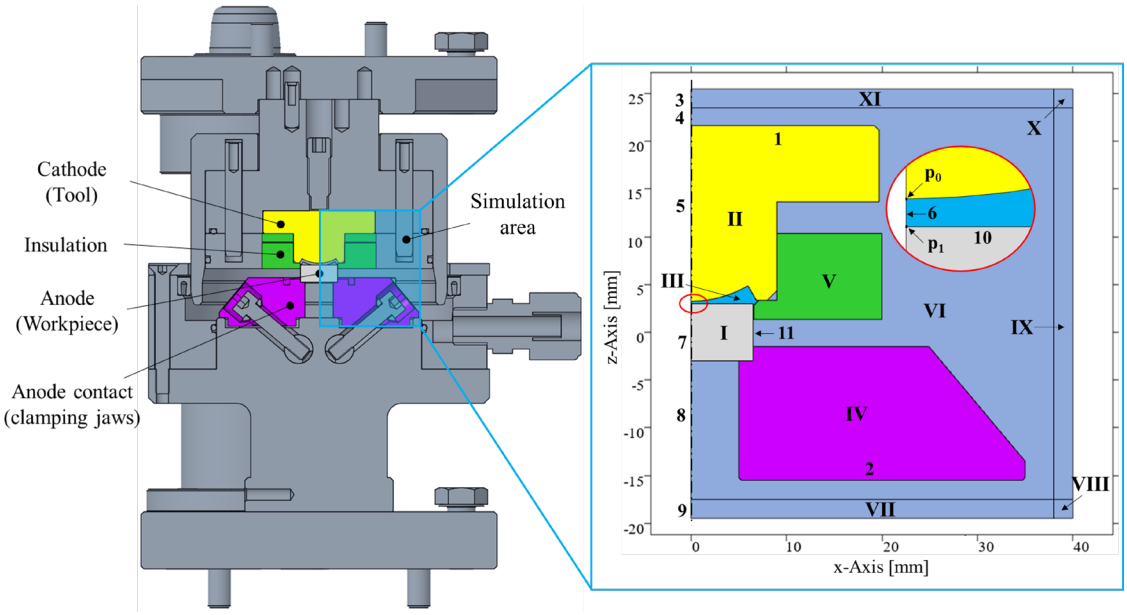

Figure 4 – Cross-section of the PECM device (left) and derived 2D model geometry (right)

The model geometry includes the domains workpiece (I), cathode (II), electrolyte (III), clamping jaws (IV) and insulation (V). For the calculation and the analysis of the induction current, it is essential to model additional air domains (VI-XI) for the realistic dispersion of the magnetic field of the workpiece. The workpiece, cathode, insulation and clamping jaw components were first imported from the 3D CAD file as a 3D model into the simulation environment and then modelled as a 2D model using a cross-section. Since all components used have symmetry, the z-symmetry plane was utilized to halve the elements and nodes of the model geometry in order to reduce computing time. The electrolyte area was added as a negative of the working gap between the cathode and the workpiece. The electrical conductivity, relative permeability and relative permittivity of the materials are defined for calculating and analyzing the electrical induction current. Table 1 allocates the materials and material parameters to the domains shown in Fig. 4.

Table 1 - Material parameters of the simulation model

Domain	Material	σ [S/m]	μ_r	ε_r
I	Nd-Fe-B/N45	$6.67 \cdot 10^5$	1.05	1.05
II	1.4301/AISI 304	$1.4 \cdot 10^6$	1.075	1
III	Electrolyte ($NaNO_3$)	7.2	0.28	1
IV	1.4305/AISI 303	$1.37 \cdot 10^6$	1.26	1
V	PEEK	10^{-10}	1	3.2
VI	Air	$3 \cdot 10^{-15}$	1	1.006

Physics and boundary conditions

In order to calculate magnetic fields and electromagnetic induction, the *Magnetic Fields* interface was assigned to all domains of the model geometry. The physical interface solves Maxwell's equations, which are formulated using the magnetic vector potential and the scalar electric potential as the dependent variables. The measurement of the remanent magnetic flux density of experimental samples was carried out using a PCE-MFM 3000 magnetic field tester from *PCE Deutschland GmbH*. The target value for calibrating the workpiece is a magnetic flux density of B_r = 0.46 T ± 5 % on the face of the workpiece.

The air domains VII-XI are defined as regions of *infinite elements*. The Infinite element domain represent a region that is stretched along the x- and z coordinate axes with the effect of approximating an infinitely large domain to ensure the realistic dispersion of the magnetic field. Further magnetic boundary conditions are summarized in Table 2.

Table 2 - Domain and boundary conditions of the Magnetic Fields interface

Domain condition	Domain	Property
Ampère´s Law I	II-XI	μ_r from material (Tab. 1)
Ampère´s Law II	I	Magnetization model: Remanent flux density B_r = 1.35 T [6] Remanent flux direction $e_X = 0; e_Y = 0; e_Z = 1$
Infinite Element Domain	VII-XI	$f(\xi) = \frac{\xi}{\gamma - \xi} \cdot \Delta_p$
Boundary condition	Boundary	Property
Axis symmetry	3-9	-

The oscillation parameters of the simulation models are summarized in Table 3.

Table 3 - Motion parameters of the cathode derived from [6]

Description	Symbol	Value	Unit
Amplitude	$\hat{z}$	0.185	[mm]
Oscillation frequency	f_z	50	[Hz]
Period	T	0.02	[s]
Initial working distance (Model initial state)	$S_{F\text{-}A}$	0.1	[mm]
End front working distance (Model final state)	$S_{F\text{-}E}$	0.085	[mm]

Oscillating components of the simulation models are the cathode (II) and the insulation unit (V). The *Moving Mesh* interface was applied to implement the oscillation of the corresponding domains. The oscillation can be described with a time-dependent cosine function as provided in Eq. 2.

$$Z(t) = \hat{z} \cdot \cos\left(2 \cdot \pi \cdot f_z \cdot t + \frac{\pi}{2}\right) \quad (2)$$

The upper and lower dead center of the cathode position during oscillation is defined by the amplitude $\hat{z}$. The oscillation frequency is f_z, from which the period time T results. To evaluate the results of the induced current, 2 periods are analyzed in this simulation study. Domain and boundary conditions of the *Moving Mesh* Interface are listed and described in Table 4.

Table 4 - Domain and boundary condition of the Moving Mesh interface

Domain condition	Domain	Property
Prescribed Deformation I	II, V	$d_x = d_y = 0$ m; $d_z = Z(t) = \hat{z} \cdot \cos\left(2 \cdot \pi \cdot f_z \cdot t + \frac{\pi}{2}\right)$
Prescribed Deformation II	I, IV, VII-XI	$d_x = d_y = d_z = 0$ m
Deforming Domain	III, VI	Initial deformation $d_x = d_y = d_z = 0$ m
Boundary condition	Boundary	Property
Prescribed Mesh Displacement in Normal Direction	4, 6, 8, 11	$d_n = 0$ m

The process input parameters of the pulsed electric potential are summarized in Table 5.

Table 5 - Pulsed electric potential parameters derived from [6]

Description	Symbol	Value	Unit
Pulse width	t_{pulse}	0.004	[s]
Pulse start	t_{start}	0.003 / 0.023	[s]
Pulse end	t_{end}	0.007 / 0.027	[s]
Process voltage	U_{min}	14	[V]

The *Electric Current* interface was applied to supply the PECM process with external electric potential. Eq. 3 was defined to integrate the pulsed voltage $U_{pulsed}(t)$ into the simulation model.

$$U_{pulsed}(t) = U_{control} \cdot U_{min} \cdot \frac{(p_0 - p_1)}{s_{F-A/E}} \tag{3}$$

$U_{control}$ is defined as a discrete variable in the *Event* interface and switches the electrical voltage on and off in the specified period time. U_{min} is calculated from the sum of all overvoltages of the boundary layers of workpiece and cathode and the voltage drop in the electrolyte solution. The value U_{min} is taken from the experiments shown [6]. The aim of PECM is to maintain a constant electrical process current. Accordingly, the electrical voltage is controlled dynamically depending on the changing working gap during the PECM process. For the PEMCenter 8000 from *PEMTec SNC* used in the experiments, 4 generators are used to provide the required electrical voltage. The control technology of the PEMCenter 8000 is realized in the simulation of the 3rd term of Eq. 3. During the transient calculation, the geometric point p_0 is tracked using a software internal probe function. The Point p_1 is a fixed point on the surface of the respective workpieces. Both points are shown in Fig. 3. The different working distances depending on the different models are $S_{F\text{-}A/E}$. The boundary conditions and variables for implementing the electrical voltage are summarized in Table 6.

Table 6 - Domain and boundary conditions of the Electric Current and the Event interfaces

Boundary condition	Boundary	Property
Electric potential	2	$U_{\mathrm{pulsed}}(t)$
Ground	1	$\varphi_{\mathrm{el}} = 0$ V
Axis symmetry	3-9	-
Event interface condition	Variable/States	Property
Discrete variable	U_{control}	0 or 1
Indicator states I	U_{start}	$t - t_{\mathrm{start}}$
Indicator states II	U_{end}	$t - t_{\mathrm{end}}$
Implicit event I	$U_{\mathrm{start}} > 0$	$U_{\mathrm{control}} = 1$
Implicit event II	$U_{\mathrm{end}} > 0$	$U_{\mathrm{control}} = 0$

The boundary conditions of the electrical voltage and the oscillation movement of the cathode are shown as graphs in Fig. 5.

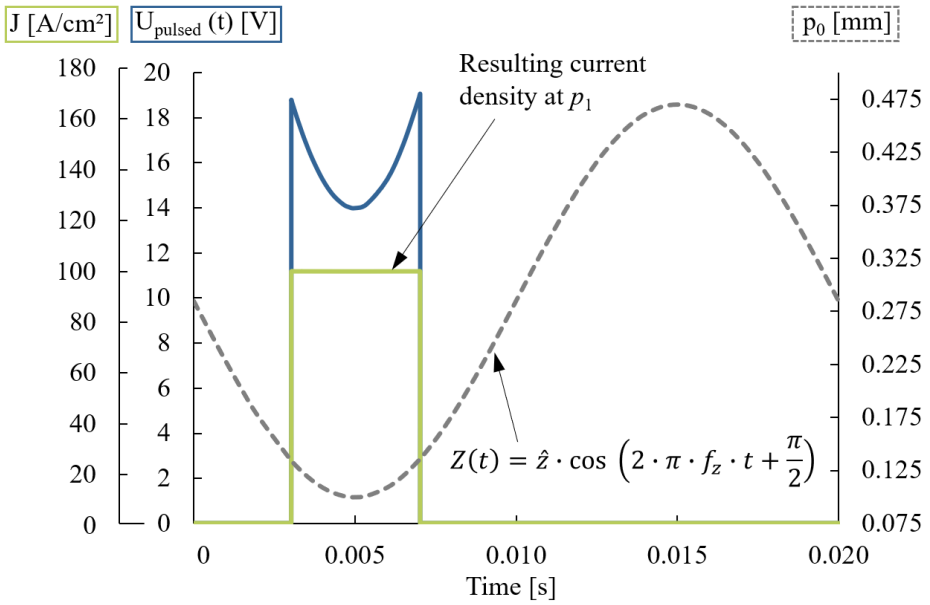

Figure 5 – Integrated boundary conditions of oscillation movement, electrical voltage and resulting current density plotted in one period

Results of the simulation

The average remanent magnetic flux density on the face of the workpiece surface in the Model initial state is $B_{\mathrm{r}} = 0.45$ T and thus within the tolerance of the remanent magnetic flux density of the measured samples. On the face of the workpiece surface in Model final state, the magnetic flux density increases to $B_{\mathrm{r}} = 0.51$ T due to the change in geometry. Fig. 6 shows the magnetic flux density in the models.

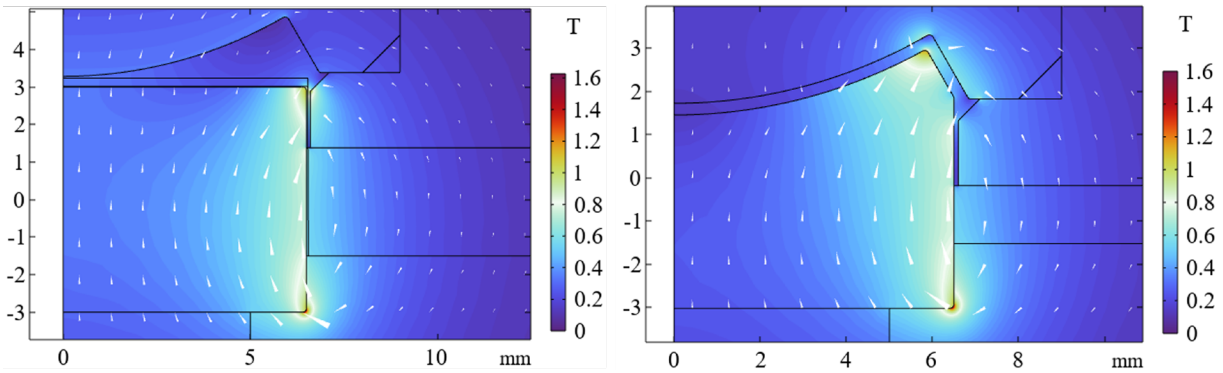

Figure 6 – False color representation of the magnetic flux density and the magnetic field lines (white cones) in Model initial state (left) and Model final state (right)

The density of the magnetic field lines increases at the workpiece corners of the north and south pole. Accordingly, the maximum magnetic flux density is localized at the corners of the workpiece and measures up to B_r = 1.6 T.

As described in Eq. 1, the oscillating movement of the cathode relative to the stationary magnetic field of the workpiece leads to an electrical current induction in the cathode and workpiece domains. Fig. 7 shows the electrical current induction in a false color representation.

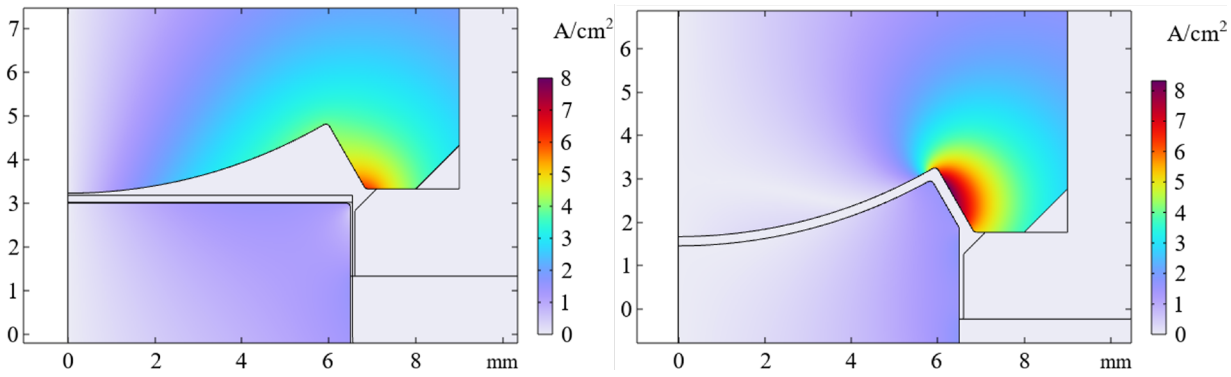

Figure 7 – Induced current density at t = 0.001 s at Model initial state (left) and Model final state (right)

A maximum induced current density of 6 A/cm² for Model initial state and 8 A/cm² for Model final state was determined in the cathode. A lower induced current of a maximum of 0.7 A/cm² in Model initial state and up to 1 A/cm² in Model final state is detected on the workpiece surface on boundary 10. The induced current is significantly lower than the current flowing due to the externally applied potential.

For comparison, Fig. 8 shows the distribution of the electrical current density with external potential in the models.

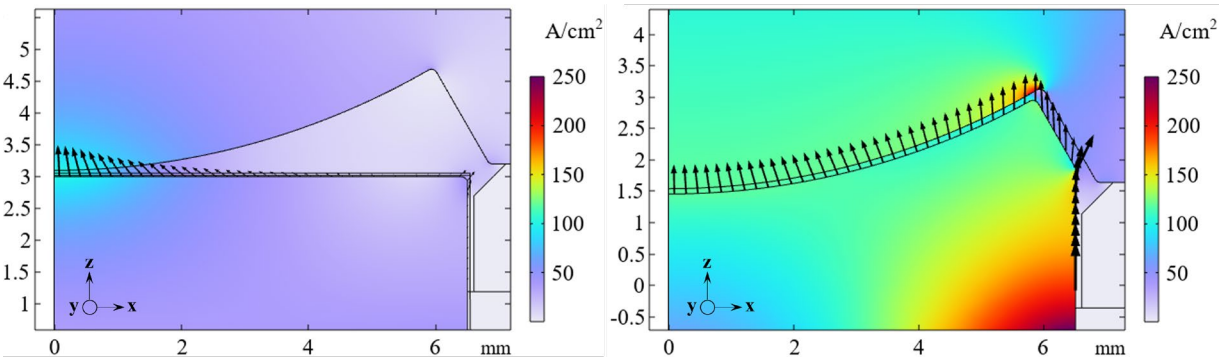

Figure 8 - False color representation of electric current density with external potential and the direction of current (black Arrows on boundary 10) at t = 0.005 s at Model initial state (left) and Model final state (right)

The high current densities of up to 250 A/cm² are caused by electrical peak effects, which are not decisive for ECM removal due to their localization in the contact area between the workpiece and the clamping jaws. The maximum current densities on the workpiece surface on boundary 10 are 100 A/cm² in Model initial state and 120 A/cm² in Model final state. In addition to the magnitudes of the electrical current density, the direction of the current is decisive for the charge transport, without which there is no removal from the workpiece in an ECM process. In the case of the applied coordinate system of the 2D models, it is necessary for the electric current to flow in the z-direction, as with the current with external potential (Fig. 8). Applying the O*ut-of-Plane* node, it is possible to extrude the 2D geometry in the y-direction in order to make the 2D equation identical to the equation used for 3D components. Fig. 9 shows the induced current in the x-direction, in the z-direction and in the extruded y-direction of the 2D models.

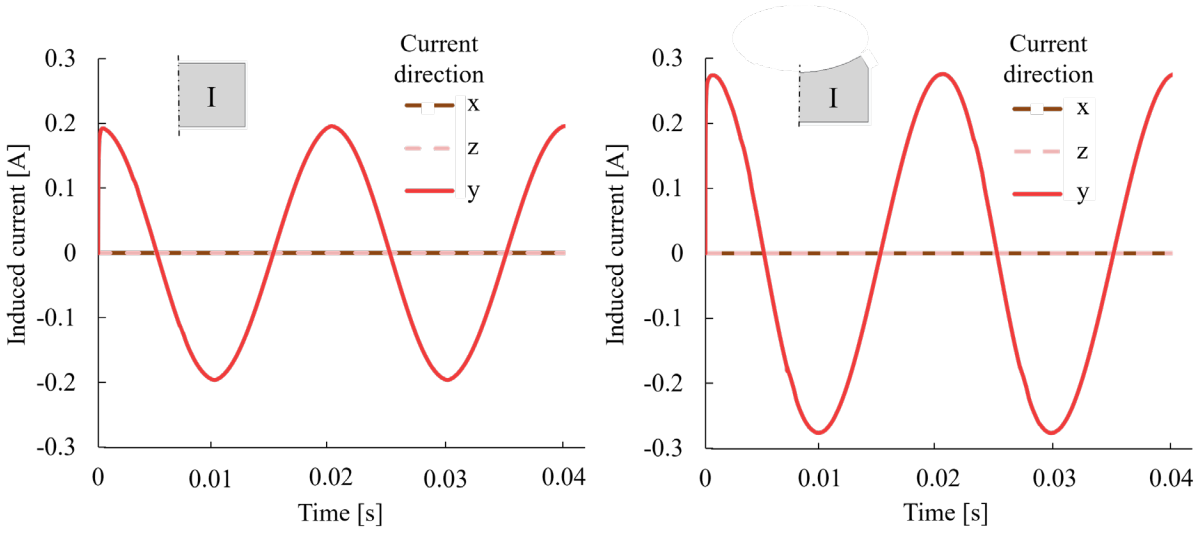

Figure 9 – Induced current direction in the workpiece (half of domain I) of Model initial state (left) and Model final state (right)

Fig. 9 shows that the induced electric current distributes in the rectangular workpiece as a circular eddy current before and during processing. Furthermore, it can be seen that the polarity of the induced current changes during the machining process as soon as the cathode has reached bottom or top dead center. Despite the induced eddy currents in the workpiece, no removal-effective charges flow in the z-direction during induction in the PECM process. The differences

between the current induced by the magnetic field of the workpiece and the oscillating cathode and the pulsed current with external potential are summarized in Table 7.

Table 7 - Summarized simulation results

Characteristic	Induction current	Pulsed current
Current type	Alternating current (AC)	Direct current (DC)
Direction of current	Circular	Straight
Current density (on workpiece surface)	Max. 1 A/cm²	Max. 120 A/cm²

Summary

In this study, 2 transient 2D models were shown for the simulation of precise electrochemical machining of a permanent magnet applying *COMSOL Multiphysics*. The simulation results show that the oscillating movement of the cathode relative to the workpiece causes an electrical induction current in the areas of the cathode and the workpiece in accordance with Faraday's law of induction. Due to the circular propagation of the induction current and the relatively low current density of a maximum of 1 A/cm² induced on the workpiece surface, it is not assumed that the induction current has an influence on the removal-effective process current. Based on this study, it is not necessary to change the process input parameters in PECM experiments if the machining strategy and magnetization of the workpieces are the same. In further studies a 3D model for further evaluation of the induced current in the PECM process will be investigated.

Acknowledgements

This project is funded by the Federal Ministry for Economic Affairs and Climate Action, following a decision of the German Bundestag.

References

[1] B. J. Smith, M. E. Riddle, M. R. Earlam, C. Iloeje, D. Diamond, "EERE Technical Report Template: Rare Earth Permanent Magnets," p. 15, 2022. [Online]. Available: https://www.energy.gov/sites/default/files/2022-02/Neodymium%20Magnets%20Supply%20Chain%20Report%20-%20Final.pdf

[2] H. Takezawa, N. Hirakawa, and N. Mohri, "Surface Magnetic Flux Density Patterning in EDM of Permanent Magnets," *Procedia CIRP*, vol. 42, pp. 668–672, 2016. https://doi.org/10.1016/j.procir.2016.02.299.

[3] A. Schubert, G. Meichsner, M. Hackert-Oschätzchen, M. Zinecker, and J. Edelmann, "Pulsed Electrochemical Machining of Powder Metallurgy Steels, 7th International Symposium on Electrochemical Machining Technology. (2011), https://doi.org/10.24406/publica-fhg-372620

[4] A. Thielecke, M. Hackert-Oschätzchen, N. Komilov, G. Meichsner, T. Petzold, S. Loebel, A. Martin, R. Schulze, and A. Schubert, "Simulation-based analysis of electrical current induction in electrochemical precision machining of Nd-Fe-B permanent magnets," *Procedia CIRP*, 2023. https://doi.org/10.1016/j.procir.2023.03.039.

[5] N. Ida, *Engineering Electromagnetics*. Cham: Springer International Publishing, 2015.

[6] A. Martin, T. Berger, S. Loebel, R. Schulze, A. Thielecke, M. Hackert-Oschätzchen, and A. Schubert, "Accuracy of pulsed electrochemical machining of NdFeB rotor magnets," in *International Symposium on Electrochemical Machining Technology 2023 (INSECT 2023)*, Saarbrücken: Center for Mechatronics and Automation Technology, 2023, 2023.